The 15th International Symposium on Magnetic Bearings, August 3-6, 2016, Mojiko Hotel, Kitakyushu, Japan

ISMB15

Advanced Control Performance in Compressor Surge

Emil KURVINEN*, Roger FITTRO** and Eric MASLEN***

* FS Dynamics Finland Oy Ab
Lars Sonckin kaari 14, 02600 Espoo, Finland

** Mechanical & Aerospace Engineering Department, University of Virginia
PO Box 400746 Charlottesville, VA 22904-4746, USA
E-mail: rlf9w@eservices.virginia.edu

*** Department of Integrated Science and Technology, James Madison University
701 Carrier Drive - ISAT 322 MSC 4102 Harrisonburg, VA 22807, USA

Abstract

Single stage compressors supported in magnetic bearings are known to exhibit compromised capacity to handle loads associated with compressor surge and stall - generally in a frequency range from about 10 Hz to 100 Hz. The present work studies utilization of advanced control in order to achieve high machine load capacity at these frequencies. A case study of a machine similar to a chiller compressor was used to study the performance with a generalized, multiple-input multiple-output (MIMO) H-infinity control with different input weighting. In the study, the machine load capacity, i.e., radial load at impeller location at different frequencies is studied. It was found that H-infinity control can achieve high machine load capacity over surge and stall frequencies (0 to 100 Hz) and in addition, it can achieve nearly the theoretical capacity limit. This type of controller enables the design of the input weighting to achieve good performance over the desired frequency range. This observation provides motive to more strongly consider advanced MIMO control methods for active magnetic bearings especially in compressor type applications.

Key words : advanced controller, compressor, machine load capacity, radial magnetic bearing, stall, surge

1. Introduction

Active magnetic bearing (AMB) supported compressors, widely used in various industries, experience two types of instabilities at low mass flows: stall and surge. In stall, the flow circulates between the vanes and in surge, the entire flow will cyclically reverse direction. These instabilities can result in high radial vibration, axial thrust displacement and temperature increase. (McMillan, 1983) The large loads associated with these instabilities can be avoided by restricting operation of the compressor well away from low mass flows. However, such an approach may excessively limit the compressor's operating range and achievable efficiency. Another approach is to use active surge/stall control to ensure stability and extend the stable regime by using feedback of pressure and flow information to the AMB controllers as presented in extensive prior literature. (Gravdahl & Egeland, 1999; Spakovszky et al., 2001; Sanadgol, 2006; Yoon et al., 2009, 2013) Unlike this prior work which aimed to actually stabilize the acoustic phenomena which lead to surge and stall, the work presented here assumes that these phenomena will not be suppressed and seeks to improve the system's ability to tolerate the radial forces they induce. Stall produces radial forces in the frequency range of 50 Hz to 100 Hz, at a fraction of the operating speed. Surge is reported to produce radial forces with frequencies ranging from 0.5 Hz to 21 Hz and is related to the compressor design and piping system. (McMillan, 1983; Greitzer, 1980; Yoon et al., 2013)

2. Approach

In this study, the use of an advanced controller is studied in a chiller compressor application. The compressor is supported via two radial magnetic bearings. In this application the manufacturer has indicated low performance related to conventional PID controlled radial magnetic bearings at low mass flow. A prior study by the authors showed that, by using more advanced bearing control, the machine load capacity could be improved significantly (Kurvinen, Fittro, & Maslen, 2016). The focus of the present study is to explore how this performance enhancement might be more specifically

tailored to the demands of surge and stall accommodation by more intentional design of the input and/or output weighting functions of the $\mathcal{H}_\infty$ control problem.

In this work, the "machine load capacity" is defined as a measure of how much load can be applied to the impeller at various frequencies before either the maximum load capacity of the AMB or the allowable clearance is exceeded. It should be noted that the machine load capacity can be easily mixed-up with load capacity, which is related to individual bearing performance. However, in the present work, the machine overall performance (machine load capacity) is studied, and this includes individual bearing load capacity as one factor. The aim is to improve the machine overall performance, which may involve improvements to bearing performance.

A common observation when using conventional PID control to control radial AMB's in compressor applications is that the machine load capacity of an AMB supported compressor is substantially lower in the frequency range of surge/stall than, for example, in response to static loads. Consequently, the need to make the machines able to tolerate surge and stall events drives designers to use bearings that are much larger than would otherwise be needed for normal operating loads.

As with the previous study, the present work examines the use of advanced AMB control algorithms to improve this machine load capacity without recourse to excessively large physical bearing components. A specific focus of the present work, extending the prior work, is to examine the influence of shaped weighting functions in the $\mathcal{H}_\infty$ design process to achieve machine load capacity more specifically tailored to the anticipated spectra of the surge and stall loads.

2.1. Rotor modelling and layout

In order to investigate the general dynamic machine load capacity performance trends, a specific representative case was chosen for analysis. The case chosen for this study is a single-stage centrifugal compressor supported with two identical radial active magnetic bearings and a thrust bearing at the end opposite to the impeller. The overall rotor weight is 108.4 kg, the length is 1.035 m and the first bending mode is at 14328.6 rpm (238.81 Hz). The maximum operating speed is 19000 rpm. The rotor for the selected case study is supercritical: the running speed is above the first bending mode of the rotor. Therefore in order to model the dynamics accurately, it is necessary to include the flexible modes in the rotor model (Lei & Palazzolo, 2008). Figure 1 depicts the overall rotor layout.

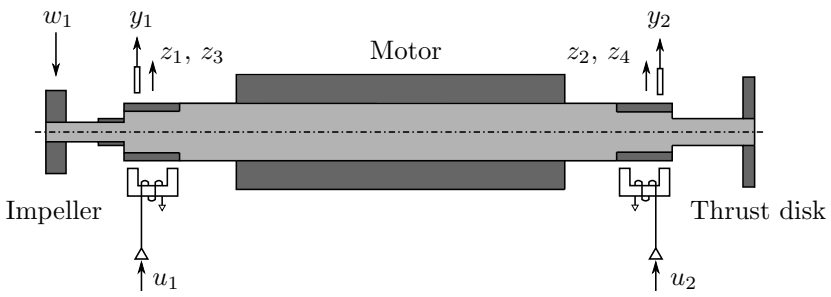

Fig. 1 Overall layout of the studied machine.

A finite element method was used to develop the model of the flexible rotor. The rotor was modeled with 95 Timoshenko beam elements. The impeller, bearing and motor laminations, and thrust disk were modeled as lumped mass elements, *e.g.*, they were assumed not to produce additional stiffness to the rotor. The model was used to produce the rotor state-space model and to calculate the free-free modes and frequencies.

In the present work, modal reduction of the rotor model was accomplished by considering the worst case response of the rotor to bounded excitation from the AMB. In this way, we do not assume that unmodelled modes are stable: we just ensure that the largest contribution to rotor response is still acceptable. The analysis proceeds from a simple I/O model of the free–free rotor:

$$\bar{z} = \bar{G}(s;\Omega,N)\bar{f} \tag{1}$$

in which $\bar{z}$ is the set of physical responses normalized by some acceptable percentage of clearance or other limiting measure, $\bar{f}$ is the set of normalized excitations including both AMB excitations and unbalance or other anticipated excitations, Ω is the rotor rotating speed, and N is the number of retained modes in the model. Here, the normalization is typically frequency dependent and this dependance is absorbed into $\bar{G}$.

The error introduced by modal reduction is, simply,

$$\bar{e}_N = \bar{z}_\infty - \bar{z}_N = \left(\bar{G}(s;\Omega,\infty) - \bar{G}(s;\Omega,N)\right)\bar{f} \tag{2}$$

The goal is to ensure that this error is not large enough to cause unmodeled contact:

$$|\bar{e}_N|_\infty \leq 1 \quad \forall \ \left|\bar{f}\right|_\infty \leq 1 \text{ and } s = j\omega : 0 < \omega < \infty \tag{3}$$

In this way, the problem of choosing the modal cut–off becomes one of minimizing N subject to this performance constraint.

The result of this analysis was a rotor model which includes six free-free modes and 1% modal damping. The six free-free mode shapes and natural frequencies of the rotor are shown in Fig. 2. Vertical lines indicate the impeller (I1), sensor (S1, S2) and bearing (B1, B2) locations. In the rotor, the radial bearing centers are located 0.147 m and 0.874 m from the impeller end and the sensors are located at 0.122 m and 0.900 m, respectively. The second flexible mode (#4) particularly exhibits the symptoms of sensor-actuator non-collocation: there is a node between the right bearing and sensor. This non-collocation reflects the fact that the sensor and actuator are separated along the rotor. The result of this "defective" mode is that the rotor transfer function has a pair of poles and zeros that are out of sequence with the consequence that the transfer function exhibits more than 180 degrees of phase lag (Bleuler et al., 2009). Such non-collocation can require notch filters in the control in order to prevent destabilizing these modes. These notch filters must be hand selected when doing PID control but are an natural feature of automatically generated MIMO controllers such as $\mathcal{H}_\infty$ or μ.

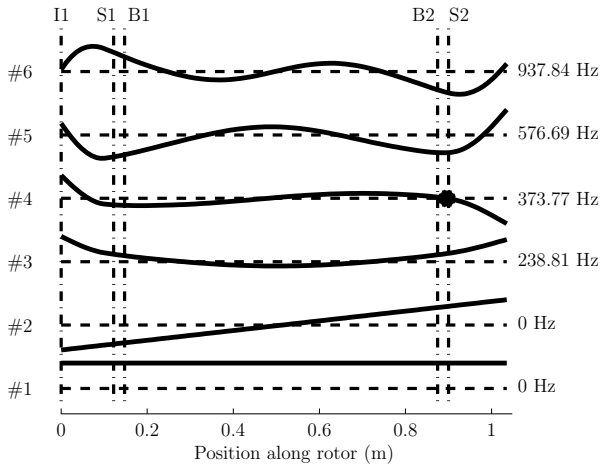

Fig. 2 Free-free mode shapes and natural frequencies of the rotor.

The general parameters for the rotor and the dynamics of the hardware are shown in Table 1.

2.2. Active Magnetic Bearings

The parameters used to calculate the magnetic bearing properties are shown in Table 2. The bearing properties are calculated from the bearing physical dimensions according to the equations presented in (Bleuler et al., 2009). The rotor state space model is appended with the magnetic bearing properties and related hardware dynamics in order to produce the overall system model. Touchdown bearings located near each AMB limit the radial rotor motion to half of the air gap length (s_0) to avoid contact with the AMB actuators.

Weighting functions are used in the $\mathcal{H}_\infty$ control design process in order to improve performance over frequencies of interest. The output weightings used in the control design were chosen to be the reciprocals of the maximum magnetic bearing force and the maximum allowable displacement (in this case half of the physical air gap length would mean contact with the touchdown bearing). This scaling choice results in normalizing the outputs of the generalized plant so that the desired normalized response of each signal is less than 1.0.

Three different input weightings were chosen with three objectives: the first was to maximize machine load capacity with a constant weighting over the full frequency spectrum, the second was to maximize machine load capacity over the surge/stall regime from 0.5 Hz to 100 Hz, and the third was to maximize machine load capacity from 0 Hz to 250 Hz. The frequency dependent input weighting has peaks over these frequency ranges, i.e., the controller is required to compensate higher forces over these frequency ranges.

Table 1 General parameters of the rotor and the dynamics

Properties	Symbol	Value
Rated speed	n_{rat}	18 000 rpm
Amplifier dc gain	K_{Adc}	2 A/V
Sensor dc gain	K_{Sdc}	40 000 V/m
Amplifier cut off frequency	f_{A}	1200 Hz
Sensor cut off frequency	f_{S}	10 000 Hz
Digital controller delay	τ	150 ms
Impeller specifications:		
Mass	m_{i}	2.8 kg
Polar mass moment of inertia	I_{p}	0.005 kgm^2
Diametral mass moment of inertia	I_{d}	0.003 kgm^2
Axial disk specifications:		
Mass	m_{i}	2.7 kg
Polar mass moment of inertia	I_{p}	0.009 kgm^2
Diametral mass moment of inertia	I_{d}	0.005 kgm^2
Material properties:		
Rotor, Impeller & Axial disk		
Elastic modulus	$E_{\mathrm{r}}, E_{\mathrm{i}}$	197 $\cdot 10^{11}$ Pa
Density	$\rho_{\mathrm{r}}, \rho_{\mathrm{i}}$	7833 kg/m^3

Table 2 Magnetic bearing specifications

Properties	Symbol	Bearing
Bearing length	l_{b}	0.075 m
Bearing diameter	d_{b},	0.085 m
Bearing saturation current	I_{s}	20 A
Pole area	A_{p}	1258.47 mm^2
Static load	F_{s}	2368.59 N
Current gain	K_{i}	236.859 N/A
Open loop stiffness	K_{x}	-4.737 $\cdot 10^6$ N/m
Inductance	L_{b}	25.64 mH
Saturation flux density	B_{s}	1.6 T
Nominal air gap length	s_0	0.5 $\cdot 10^{-3}$ m

2.3. Control system and weighting functions

Figure 3 depicts the generalized state-space plant model used for the $\mathcal{H}_\infty$ control design. The state-space model includes the physical rotor model and the dynamics of the amplifier, sensor, and controller delay. The delay is modeled with a third order Padé approximation (Bleuler et al., 2009). In the generalized form, weighting functions for disturbances and performance measures are also included (Skogestad & Postlethwaite, 2007). Details of the weighting functions are discussed below. For the generalized plant model, the control design is developed via a standard MATLAB (MATLAB, 2013) function. With the designed controller, the closed loop transfer function was then built, and the resulting performance was analyzed.

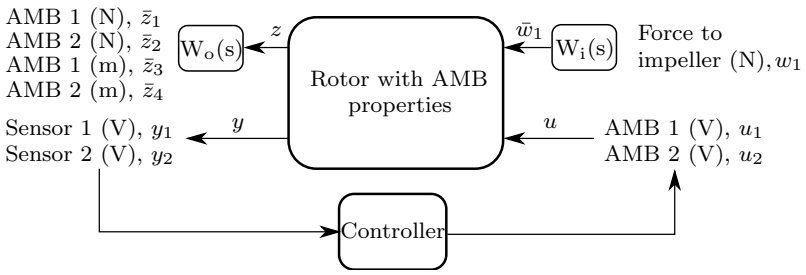

Fig. 3 Plant model with input and output weightings.

The output weightings ($W_O(s)$) used in the control design were chosen to be the reciprocals of the maximum magnetic bearing force and the maximum allowable displacement (in this case half of the physical air gap length would mean contact with the touchdown bearing). This scaling choice results in normalizing the outputs of the generalized plant so that the desired normalized response of each signal is less than 1.0.

The input weighting ($W_i(s)$) is selected in order to maximize machine load capacity over the desired frequency range. Figure 4 depicts the different input weightings used in the study. The first of them is a constant 890 N at all frequencies meaning that the controller is required to compensate constant force over the full studied frequency range. The second aims to maximize the machine load capacity from zero to 100 Hz and has a peak over this frequency range in order to compensate higher forces over this frequency range. The third aims to maximize machine load capacity from zero to 250 Hz and has a higher but almost constant force up to 165 Hz and decreases after that. The input weightings are iteratively tuned, in order to achieve the highest machine load capacity over the desired frequency range.

As a point of comparison, the theoretical maximum physical machine load capacity was calculated. Limiting performance in Fig. 5 refers to this theoretical upper bound for the attainable performance that takes the actuator hardware and the rotor dynamic behavior into account but does not include the feeback control law. Further, this prior study also examined the performance attainable using conventional PID control. (Kurvinen et al., 2016)

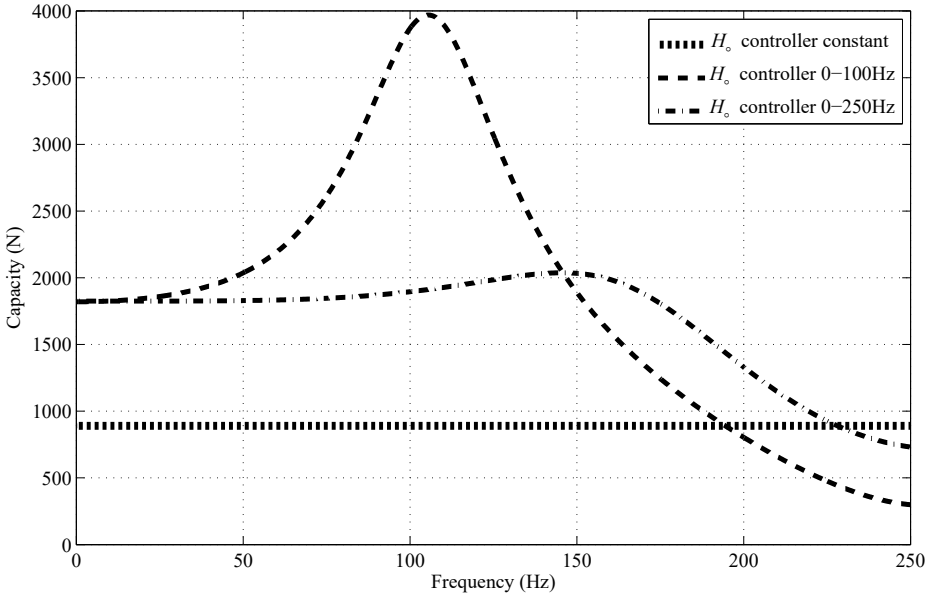

Fig. 4 Input weighting functions used in the studied cases.

3. Results

Figure 5 depicts the calculated machine load capacities with the input weightings shown in Fig. 4, and for a comparison from the previous study (Kurvinen et al., 2016), the attainable machine load capacity with decentralized PID controller.

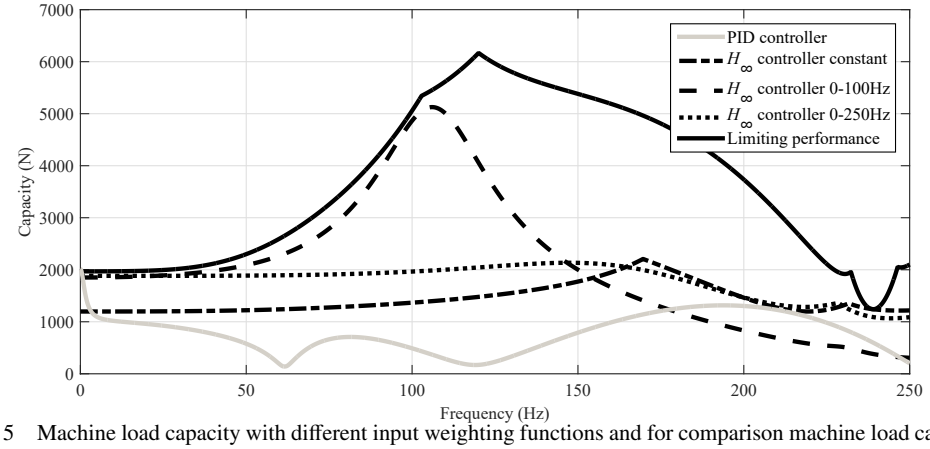

Fig. 5 Machine load capacity with different input weighting functions and for comparison machine load capacity with first order decentralized PID controller. Note the use of linear-linear scales.

With the constant input weighting, the machine load capacity at steady state is 1200 N radial load at the impeller location. It rises steadily up to 170 Hz where the peak of 2200 N is achieved and decreases close to the steady state capacity at the maximum 250 Hz frequency.

With the input weighting that aims to maximize the machine load capacity over the surge and stall frequency range (0 to 100 Hz), the result closely follows the limiting performance capacity and yields a very high peak of 5100 N machine load capacity. However, above 100 Hz, the machine load capacity begins to diminish and demonstrates lower performance, with the constant input weighting above 155 Hz.

With the input weighting that aims to maximize the performance from zero to 250 Hz, the load capacity at low frequency is near the limiting performance and yields almost constant machine load capacity up to 165 Hz and above that range the machine load capacity is similar to that obtained with the constant input weighting.

With constant input weighting, the machine load capacity is lower than with the two others that aimed for high machine load capacity over a relatively narrow frequency range. This is because the controller is attempting to have good performance at all possible frequencies.

When it is not necessary to have good load management over part of the spectrum (for instance, at high frequencies where no loads are expected), it is possible to substantially enhance the load management over other parts of the spectrum (for instance, between 0 and 150 Hz). Such trade-offs are natural and recognizing that un-needed capacity at high frequencies always comes at the expense of capacity at low frequencies can help the design engineer extract performance that would otherwise appear to be impossible. The value of $\mathcal{H}_\infty$ control in this setting is that it enables such tradeoffs to be built into the design process explicitly.

One observation that is particularly apparent is that the machine load capacity using almost any of these methods is always better than what can be achieved with PID control. The highly tuned $\mathcal{H}_\infty$ control shows lower machine load capacity than with PID at frequencies beyond 170 Hz, but this range is also well beyond the typical load spectrum associated with surge and stall phenomena.

4. Conclusions

As previously demonstrated in (Kurvinen et al., 2016), the need to recover substantial load capacity in the frequency ranges associated with surge and stall provides strong motivation to consider MIMO design processes like $\mathcal{H}_\infty$ or perhaps μ. An important feature of any of these design methods is the ability to shape the input and output weighting functions. The work reported here shows that shaping the input weighting function to focus control effort on the range of frequencies associated with surge and stall can lead to controllers that achieve machine capacities not only substantially better than those achieved with PID control but also better than those achieved with flat weighting in $\mathcal{H}_\infty$ control.

These improvements are not at all marginal: they can readily represent improvements on the order of 5 or 6 times the performance obtained with more conventional control without any need to increase actuator magnetic capacity. In such a case, the economic benefit to the more sophisticated (read: complicated) control may be very easy to justify and, in many cases, may make the application possible.

References

Bleuler, H., Cole, M., Keogh, P., Larsonneur, R., Maslen, E., Okada, Y., Schweitzer, G., & Traxler, A. (2009). *Magnetic bearings: Theory, design, and application to rotating machinery* (First ed.). Berlin Heidelberg: Springer Science & Business Media. doi: 10.1007/978-3-642-00497-1

Cloud, H., Li, G., Barrett, L. E., Foiles, W. C., & Maslen, E. H. (2005). Practical applications of singular value decomposition in rotordynamics. *Australian Journal of Mechanical Engineering*, *2*(1), 21-32.

Gravdahl, J. T., & Egeland, O. (1999). *Compressor surge and rotating stall: Modeling and control* (First ed.). London: Springer-Verlag. doi: 10.1007/978-1-4471-0827-6

Greitzer, E. M. (1980). Review - axial compressor stall phenomena. *Journal of Fluids Engineering*, *102*, 134–151. doi: 10.1115/1.3240634

Kurvinen, E., Fittro, R., & Maslen, E. (2016). Improving compressor surge performance with advanced control. *Proceedings of the Institution of Mechanical Engineers, Part I: Journal of Systems and Control Engineering*, *Prepublished May, 9th, 2016*, 1–8. doi: 10.1177/0959651816647557

Lei, S., & Palazzolo, A. (2008). Control of flexible rotor systems with active magnetic bearings. *Journal of Sound and Vibration*, *314*(1), 19–38. doi: 10.1016/j.jsv.2007.12.028

MATLAB. (2013). *R2013a (8.1.0.604)*. Natick, Massachusetts: The MathWorks Inc.

McMillan, G. (1983). *Centrifugal and axial compressor control* (First ed.). Research Triangle Park, NC: Instrument Society of America.

Sanadgol, D. (2006). *Active control of surge in centrifugal compressors using magnetic thrust bearing actuation* (Dissertation). University of Virginia.

Skogestad, S., & Postlethwaite, I. (2007). *Multivariable feedback control: Analysis and design* (second ed., Vol. 2). New York: John Wiley & Sons.

Spakovszky, Z., Paduano, J., Larsonneur, R., Traxler, A., & Bright, M. (2001). Tip clearance actuation with magnetic bearings for high-speed compressor stall control. *Journal of Turbomachinery*, *123*(3), 464–472. doi: 10.1115/2000-GT-0528

Yoon, S. Y., Lin, Z., & Allaire, P. E. (2013). *Control of surge in centrifugal compressors by active magnetic bearings: Theory and implementation* (First ed.). London: Springer-Verlag. doi: 10.1007/978-1-4471-4240-9

Yoon, S. Y., Lin, Z., Lim, K. T., Goyne, C., & Allaire, P. E. (2009). Model validation for an amb-based compressor surge control test rig. In *Decision and control, 2009 held jointly with the 2009 28th chinese control conference. cdc/ccc 2009. proceedings of the 48th ieee conference on* (pp. 756–761). doi: 10.1109/CDC.2009.5400567